Constitutive models for linear compressible viscoelastic flows of simple liquids at nanometer length scales ⊘

Debadi Chakraborty; John E. Sader

Check for updates

CrossMark

View Online   Export Citation

Constitutive models for linear compressible viscoelastic flows of simple liquids at nanometer length scales

Debadi Chakraborty and John E. Sader[a)]
School of Mathematics and Statistics, The University of Melbourne, Parkville, Victoria 3010, Australia

Simple bulk liquids such as water are commonly assumed to be Newtonian. While this assumption holds widely, the fluid-structure interaction of mechanical devices at nanometer scales can probe the intrinsic molecular relaxation processes in a surrounding liquid. This was recently demonstrated through measurement of the high frequency (20 GHz) linear mechanical vibrations of bipyramidal nanoparticles in simple liquids [Pelton *et al.*, "Viscoelastic flows in simple liquids generated by vibrating nanostructures," Phys. Rev. Lett. **111**, 244502 (2013)]. In this article, we review and critically assess the available constitutive equations for compressible viscoelastic flows in their linear limits—such models are required for analysis of the above-mentioned measurements. We show that previous models, with the exception of a very recent proposal, do not reproduce the required response at high frequency. We explain the physical origin of this recent model and show that it recovers all required features of a linear viscoelastic flow. This constitutive equation thus provides a rigorous foundation for the analysis of vibrating nanostructures in simple liquids. The utility of this model is demonstrated by solving the fluid-structure interaction of two common problems: (1) a sphere executing radial oscillations in liquid, which depends strongly on the liquid compressibility and (2) the extensional mode vibration of bipyramidal nanoparticles in liquid, where the effects of liquid compressibility are negligible. This highlights the importance of shear and compressional relaxation processes, as a function of flow geometry, and the impact of the shear and bulk viscosities on nanometer scale flows. © 2015 AIP Publishing LLC. [http://dx.doi.org/10.1063/1.4919620]

I. INTRODUCTION

Miniaturization of mechanical sensors to nanometer length scales affords a tremendous enhancement in their responsivity to environmental effects.[1–14] For example, a 10-fold reduction in the size of the sensor yields a 10 000-fold increase in the responsivity of its resonant frequency to mass adsorption. This strong scaling law underpins the recent demonstration of atomic-scale mass measurements using nanomechanical sensors.[15–18] Importantly, such measurements monitor the resonance properties of the sensor, which can be directly affected by any surrounding fluid. This is particularly relevant to biological applications that are inherently conducted in a fluid environment. Consequently, an ability to theoretically predict and model the performance of such fluid-structure interactions is essential for their proper design and application.

The dynamic response of mechanical structures can be strongly modified by their immersion in fluid. It is known that macroscopic structures are weakly affected by the viscosity of the surrounding fluid, with structural and acoustic radiation damping being dominant.[19] Miniaturization to micron length scales increases the resonant frequency of these devices. Scaling analysis then reveals that such a size reduction strongly enhances the effects of viscosity—this typically dominates all other damping mechanisms, especially for microelectromechanical systems and atomic force microscope

---

a)Author to whom correspondence should be addressed. E-mail: jsader@unimelb.edu.au

cantilevers.[20–22] Calculations of such fluid-structure interactions have been performed widely and display excellent agreement with measurements in both gas and liquid.[20,23]

Miniaturization of mechanical devices to nanometer length scales can dramatically change the nature of the flows they generate. Because the mean free path of a gas is at the 10-100 nm scale, immersion of nanomechanical devices in gases can intrinsically generate non-continuum flows—this property obviates use of the Navier-Stokes equations.[24] Immersion of such devices in liquid, however, does not produce non-continuum flows because the molecular length scales of liquids are orders-of-magnitude smaller than the device dimensions. This would appear to indicate that the Navier-Stokes equations are widely applicable to such small-scale flows. However, recent measurements of the vibration of gold nanoparticles (~30 nm in diameter) immersed in simple liquids (glycerol-water mixtures) have shown distinct differences with the predictions of the Navier-Stokes equations. Specifically, as the liquid viscosity was systematically increased, the quality factor (scaled inverse damping) of the resonating nanoparticles was observed to initially decrease but then plateau to a near constant value (and even increase slightly); numerical simulations based on the Navier-Stokes equations predict a strong monotonic decrease in quality factor with increasing viscosity, which was not observed. These observations were found to quantitatively agree with independent calculations that include the intrinsic viscoelastic nature of these simple liquids, with the short time scale of vibration (~50 ps) being comparable to the molecular relaxation time of the liquid. The viscoelastic properties of simple liquids must therefore be included in theoretical/experimental design and characterization of nanometer sized mechanical devices.

Flow generated by the extensional mode vibrations of the nanoparticles in Ref. 25 was well modeled using an incompressible linear Maxwell model. Justification for this choice of an incompressible constitutive equation is given by the shear-dominated nature of the flow. On the other hand, fluid compressibility is expected to play a significant role for breathing mode vibrations, which spheres exhibit predominantly.[17,26–28] It is thus critically important to include the effects of both liquid compressibility and their viscoelastic nature in the simulation of their dynamic response in simple liquids, like water.

The simplest constitutive equation for an *incompressible* viscoelastic fluid is the linear Maxwell model,[29]

$$\mathbf{S} + \lambda \frac{\partial \mathbf{S}}{\partial t} = 2\mu \mathbf{D}, \tag{1}$$

where $\mathbf{S}$ is the deviatoric stress tensor, μ is the fluid shear viscosity, λ is the relaxation time, and $\mathbf{D}$ is the rate-of-strain tensor. The linear limit is considered because the above-mentioned measurements operate in this regime.[25,30] A more general linear incompressible constitutive equation is Jeffreys' model (linear limit of the Oldroyd-B model),[31]

$$\mathbf{S} + \lambda_1 \frac{\partial \mathbf{S}}{\partial t} = 2\mu_0 \left(\mathbf{D} + \lambda_2 \frac{\partial \mathbf{D}}{\partial t} \right), \tag{2a}$$

where λ_1 is the relaxation time, λ_2 is the retardation time, and μ_0 is the zero shear-rate viscosity of the fluid. These models are often used to characterize the behavior of complex fluids, such as polymeric liquids, for which it is a common practice to separate the contributions of the Newtonian solvent and polymer in the fluid solution.[31] Following this theoretical framework, we thus recast Eq. (2a) as

$$\mathbf{S} = 2\mu_s \mathbf{D} + \mathbf{S}^P \quad \text{and} \quad \mathbf{S}^P + \lambda_1 \frac{\partial \mathbf{S}^P}{\partial t} = 2\mu_P \mathbf{D}, \tag{2b}$$

where $\mu_s = \lambda_2 \mu_0 / \lambda_1$ and $\mu_p = (1 - \lambda_2/\lambda_1) \mu_0$, with $\mu_0 = \mu_s + \mu_p$.

Again drawing on the polymeric liquid literature, we note that several constitutive models for *compressible* viscoelastic liquids have been proposed.[32–38] These models exhibit different mathematical forms, and thus, it is currently unclear which model should be used to analyze the above-mentioned nanoscale flows. A primary aim of this article is to assess the relative merits of these constitutive equations and thus to identify which model should be used in this context.

Some of these models implicitly assume a zero bulk viscosity and only include the appropriate compressible term in the rate-of-deformation tensor.[33,36] In contrast, other models include a nonzero

bulk viscosity term in the solvent contribution, which is neglected in the polymeric component.[34,37] Removal of the bulk viscosity in the polymeric equation has been related to the restriction imposed by nonequilibrium thermodynamics.[32] Strikingly, none of the models in Refs. [32–37] capture the required response in the high frequency limit, as we shall discuss. Furthermore, these models do not consider the compressional relaxation spectrum of the fluid, which in general will differ from the shear relaxation properties.[36,37] Both the shear and compressional relaxation processes collectively influence the mechanical response of a pressure wave in a viscoelastic medium. In a very recent work,[38] a mathematical modification to the incompressible linear Maxwell model was proposed to account for fluid compressibility—a primary focus of that study was to mathematically prove that the proposed constitutive equation is compatible with the Newtonian flow. However, the physical origin of the model, its derivation and connection to classical thermodynamic results were not discussed.

In this article, we elucidate the underlying physical picture and derive the constitutive equation of Ref. [38]. We also show that it recovers (i) the required classical thermodynamic results[39] and (ii) the correct response in the high frequency limit—this is in direct contrast to all other available models for compressible viscoelastic flows.[32–37] Consequently, the constitutive equation of Ref. [38] provides a rigorous foundation to simulate the compressible fluid-structure interaction of nanomechanical devices in simple liquids[25] which intrinsically probe the viscoelastic nature of these liquids. We apply this compressible constitutive equation[38] to two examples: (i) the breathing mode vibration of a sphere,[30] which generates a highly compressible flow and (ii) the extensional vibration of the bipyramidal rod-like particle,[26] which is expected to give a predominantly incompressible flow, to show the general utility of this formulation. These fluid-structure examples are commonly measured in practice,[30] and the solutions given here provide a foundation for interpretation of these measurements.

II. CONSTITUTIVE EQUATIONS FOR A COMPRESSIBLE VISCOELASTIC FLUID

We begin by briefly reviewing the conservation equations for a general fluid. Throughout, we assume that the flow exhibits small-amplitude oscillations so that all convective terms can be ignored.[21] This is the practical case[30] and enables linearization of the equations of motion.[21,40] The required linear conservation equations are

$$\frac{\partial \rho}{\partial t} + \boldsymbol{\nabla} \cdot (\rho \mathbf{v}) = 0, \quad \rho \frac{\partial \mathbf{v}}{\partial t} = \boldsymbol{\nabla} \cdot \mathbf{T}, \tag{3}$$

where $\mathbf{v}$ is the fluid velocity field and ρ is the fluid density. The Cauchy stress tensor is $\mathbf{T} = -p\mathbf{I} + \mathbf{S}$, where $\mathbf{S}$ is the deviatoric stress tensor, p is the thermodynamic pressure, and $\mathbf{I}$ is the identity tensor. The dilatation of a fluid element, $\boldsymbol{\nabla} \cdot \mathbf{v}$, together with the bulk viscosity relates the mechanical pressure, p_m, to the thermodynamic pressure, $p_m = p - \mu_B (\boldsymbol{\nabla} \cdot \mathbf{v})$, where μ_B is the fluid bulk viscosity.[41] For an incompressible fluid, $\boldsymbol{\nabla} \cdot \mathbf{v} = 0$, thus the mechanical and thermodynamic pressures are identical.

Thermodynamic pressure and fluid density are related by the equation-of-state for the fluid, which in its linear form is[39]

$$\rho = \rho_0 (1 + \kappa p), \tag{4}$$

where $\kappa = \rho_0^{-1}(\partial \rho / \partial p)$ is the fluid compressibility and ρ_0 is the fluid density at equilibrium. Substituting Eq. (4) into Eq. (3), we obtain the following linearized governing equations:

$$\frac{\partial p}{\partial t} + \kappa^{-1} \boldsymbol{\nabla} \cdot \mathbf{v} = 0, \quad \rho_0 \frac{\partial \mathbf{v}}{\partial t} = \boldsymbol{\nabla} \cdot \mathbf{T}. \tag{5}$$

For a compressible Newtonian fluid,[42] the Cauchy stress tensor is $\mathbf{T} = -p\mathbf{I} + \mathbf{S}_{sh} + \mathbf{S}_{comp}$, where $\mathbf{S}_{sh} = 2\mu \{\mathbf{D} - (\operatorname{tr}\mathbf{D})\,\mathbf{I}/3\}$ and $\mathbf{S}_{comp} = \mu_B (\operatorname{tr}\mathbf{D})\,\mathbf{I}$ are the shear and compressional contributions to the deviatoric stress tensor, respectively, μ is the fluid shear viscosity, and $\mathbf{D} = \left(\boldsymbol{\nabla}\mathbf{v} + (\boldsymbol{\nabla}\mathbf{v})^T\right)/2$ is the rate-of-strain tensor. This standard Newtonian constitutive equation is easily generalized to account for both the shear and compressional relaxation behaviors of a linear viscoelastic fluid. Considering the physical model of a spring-dashpot connected in series, for each of the shear and compressional contributions, as illustrated in Fig. 1, immediately leads to the following generalization
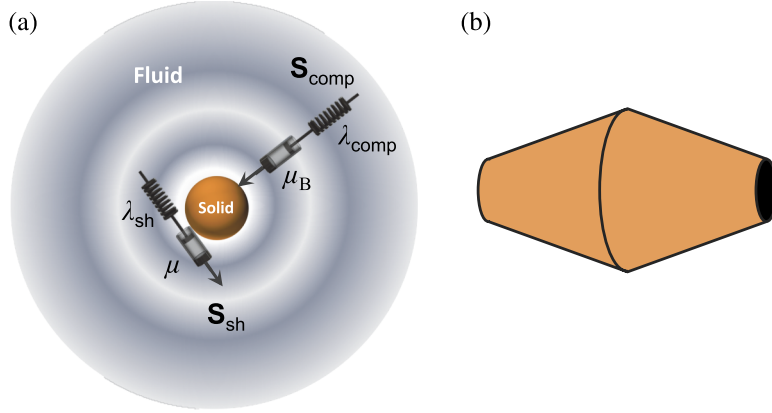
FIG. 1. Schematic of (a) viscoelastic compressional and shear components of the fluid stress acting on a vibrating solid spherical particle and (b) a bipyramidal particle.

to the Newtonian model:

$$\mathbf{S}_{\text{sh}} + \lambda_{\text{sh}}\frac{\partial \mathbf{S}_{\text{sh}}}{\partial t} = 2\mu\left(\mathbf{D} - \frac{\text{tr}\,\mathbf{D}}{3}\mathbf{I}\right), \quad \mathbf{S}_{\text{comp}} + \lambda_{\text{comp}}\frac{\partial \mathbf{S}_{\text{comp}}}{\partial t} = \mu_{\text{B}}\left(\text{tr}\,\mathbf{D}\right)\mathbf{I}, \tag{6}$$

where λ_{sh} is the shear relaxation time of the fluid and λ_{comp} is its compressional relaxation time. Equation (6) is identical to the model of Ref. 38 and is the required result that implicitly accounts for both shear and compressional relaxation effects, while giving a purely Newtonian result in the low frequency limit and a purely elastic response in the corresponding high frequency limit; see below. Use of Eqs. (5) and (6), together with the appropriate fluid boundary conditions, allows for characterization of the compressible viscoelastic response of simple liquids.

A. Comparison to classical thermodynamic result

Throughout, we assume the implicit time dependence of $e^{-i\omega t}$ for all variables, where ω is the angular frequency. According to Landau and Lifshitz,[39] a slow process that tends to establish equilibrium displays a frequency dependent relationship between the mechanical and thermodynamic pressures, i.e., $p_{\text{m}} = p - \left(c_\infty^2 - c_0^2\right)\rho_0\lambda\left(\mathbf{\nabla}\cdot\mathbf{v}\right)/\left(1 - i\omega\lambda\right)$, where λ is the relaxation time, $c_0 = 1/\sqrt{\rho_0\kappa}$ is the speed of sound in the fluid at thermodynamic equilibrium, and c_∞ is the speed of sound at very high frequency. The bulk viscosity of the fluid at thermodynamic equilibrium is related by $\mu_B = \left(c_\infty^2 - c_0^2\right)\rho_0\lambda$. Critically, we find precisely the same expression upon taking the trace of the stress tensor in Eq. (6), i.e., $p_{\text{m}} = p - \mu_{\text{B}}\left(\mathbf{\nabla}\cdot\mathbf{v}\right)/\left(1 - i\omega\lambda_{\text{comp}}\right)$.

Landau and Lifshitz[39] derived this relation between the thermodynamic and mechanical pressures to illustrate the importance of slow processes. However, they did not derive a general constitutive equation for a compressible viscoelastic fluid. The above analysis shows that the constitutive model in Eq. (6) is entirely consistent with this classical thermodynamic result of Landau and Lifshitz[39] and correctly identifies the compressional relaxation time.

It is common in experiments to report a frequency dependent speed of sound in a fluid medium.[43] This can also be derived using Eq. (6). Considering an adiabatic process, this leads to the following expression for the frequency dependent speed of sound: $c^* = c_0\left[1 - i\omega\mu_{\text{B}}/\left\{c_0^2\rho_0\left(1 - i\omega\lambda_{\text{comp}}\right)\right\}\right]^{1/2}$. Again, this is in precise agreement with Landau and Lifshitz[39] for the speed of sound for slow compressible processes, thus also supporting the validity of the constitutive equation in Eq. (6). Other constitutive models in Table I do not yield these thermodynamic results, as we now discuss.

A comparison of the constitutive equation, Eq. (6),[38] to those proposed in Refs. 32–37 for compressible viscoelastic flows is given in Table I. This shows that the constitutive models exhibit significantly different mathematical forms. To gain insight into their various properties, in Table II, we provide their asymptotic behavior in the limits of low and high normalized frequencies, $\omega\lambda$, corresponding to expected fluid-like and solid-like behaviors. At low frequency, we observe that

TABLE I. List of available constitutive models for linear compressible viscoelastic fluid flows.

Model	Deviatoric stress tensor	Additional stress tensors
Reference 32	$\mathbf{S} = \mathbf{S}^{P} - \frac{\mathrm{tr}(\mathbf{S}^{P})}{3}\mathbf{I}$	$\mathbf{S}^{P} + \lambda_1 \frac{\partial \mathbf{S}^{P}}{\partial t} = 2\mu \mathbf{D}$
References 33 and 36	$\mathbf{S} = 2\mu_{\mathrm{s}}\left(\mathbf{D} - \frac{\mathrm{tr}\,\mathbf{D}}{3}\mathbf{I}\right) + \mathbf{S}^{P}$	$\mathbf{S}^{P} + \lambda_1 \frac{\partial \mathbf{S}^{P}}{\partial t} = 2\mu_{\mathrm{P}}\left(\mathbf{D} - \frac{\mathrm{tr}\,\mathbf{D}}{3}\mathbf{I}\right)$
Reference 34	$\mathbf{S} = 2\mu_{\mathrm{s}}\left(\mathbf{D} - \frac{\mathrm{tr}\,\mathbf{D}}{3}\mathbf{I}\right) + \mu_{\mathrm{B}}(\mathrm{tr}\,\mathbf{D})\mathbf{I} + \mathbf{S}^{P}$	$\mathbf{S}^{P} = 2\mu_{\mathrm{P}}\mathbf{D}$
Reference 35	$\mathbf{S} = -2\mu \frac{\mathrm{tr}\,\mathbf{D}}{3}\mathbf{I} + \mathbf{S}^{P}$	$\mathbf{S}^{P} + \lambda_1 \frac{\partial \mathbf{S}^{P}}{\partial t} = 2\mu \mathbf{D}$
Reference 37	$\mathbf{S} = 2\mu_{\mathrm{s}}\left(\mathbf{D} - \frac{\mathrm{tr}\,\mathbf{D}}{3}\mathbf{I}\right) + \mu_{\mathrm{B}}(\mathrm{tr}\,\mathbf{D})\mathbf{I} + \mathbf{S}^{P}$	$\mathbf{S}^{P} + \lambda_1 \frac{\partial \mathbf{S}^{P}}{\partial t} = 2\mu_{\mathrm{P}}\mathbf{D}$
Equation (6) and Ref. 38	$\mathbf{S} = \mathbf{S}_{\mathrm{sh}} + \mathbf{S}_{\mathrm{comp}}$	$\mathbf{S}_{\mathrm{sh}} + \lambda_{\mathrm{sh}} \frac{\partial \mathbf{S}_{\mathrm{sh}}}{\partial t} = 2\mu\left(\mathbf{D} - \frac{\mathrm{tr}\,\mathbf{D}}{3}\mathbf{I}\right)$ $\mathbf{S}_{\mathrm{comp}} + \lambda_{\mathrm{comp}} \frac{\partial \mathbf{S}_{\mathrm{comp}}}{\partial t} = \mu_{\mathrm{B}}(\mathrm{tr}\,\mathbf{D})\mathbf{I}$

all models display a linear dependence on the rate-of-strain tensor, but some assume a zero bulk viscosity (models in Refs. 33 and 36). Interestingly, the models in Refs. 32–37 all implicitly set the compressional relaxation time of the fluid to zero. This contrasts to Eq. (6) for which both shear and compressional relaxations exist, as does the bulk fluid viscosity. In the high frequency limit, stronger deviations are evident, where a pure elastic solid response is required. All models in Refs. 32–37 predict "fluid-like" behavior with the deviatoric stress tensor remaining proportional to the rate-of-strain—or equivalently out-of-phase with the strain tensor. This is certainly not indicative of the response of an elastic solid. In striking contrast, Eq. (6) intrinsically predicts that the stress is proportional to and in-phase with the strain in the fluid—precisely the required behavior of an elastic solid. More so, the asymptotic result in Table II is immediately recognizable as Hooke's law for a linearly elastic solid with the bulk and shear moduli evident.

Table II also lists the difference between the thermodynamic and mechanical pressures predicted by the different models. Models that use a zero bulk viscosity implicitly assume no difference between these pressures. All other models correctly exhibit the required low frequency behavior. However, only the model in Eq. (6) correctly captures the required thermodynamic result of Landau and Lifshitz[39] at all frequencies. In the high frequency limit, Eq. (6) again correctly predicts that $p_{\mathrm{m}} - p$ is in-phase with the fluid displacement, not the velocity. Equation (6) also captures the correct complex speed as a function of frequency, as discussed above, in contrast to all other models. The model in Ref. 34 is derived for steady flow only.

This comparison shows that the constitutive equations in Refs. 32–37 are unable to describe the expected and pertinent features of linear compressible viscoelastic flows at high frequency, which is critical for analyzing fluid-structure interactions at nanometer scales. The only model that captures the correct behavior is Eq. (6).[38]

TABLE II. Comparison of features of linear constitutive models in Table I at low and high normalized frequencies, with bulk elastic modulus, $K = \mu_{\mathrm{B}}/\lambda_{\mathrm{comp}}$ and shear elastic modulus, $G = \mu/\lambda_{\mathrm{sh}}$. The rate-of-strain tensor, $\mathbf{D}$, and the strain tensor, $\mathbf{E}$, are related by $\mathbf{D} = -i\omega\mathbf{E}$. Note that all models in Refs. 32–37 assume a zero compressional relaxation time, i.e., $\lambda_{\mathrm{comp}} = 0$, whereas Refs. 33 and 36 also assume a zero bulk viscosity, μ_{B}. The models in Refs. 33, 34, 36, and 37 define $\mu = \mu_{\mathrm{s}} + \mu_{\mathrm{p}}$, where μ_{s} and μ_{p} are the viscosities of the Newtonian solvent and the polymer, respectively.

Model	Newtonian limit ($\omega\lambda \to 0$)	High frequency limit ($\omega\lambda \to \infty$)	$p_{\mathrm{m}} - p$
Reference 32	$\mathbf{S} = 2\mu\left(\mathbf{D} - \frac{\mathrm{tr}\,\mathbf{D}}{3}\mathbf{I}\right)$	$\mathbf{S} = \frac{2\mu}{\lambda_1}\left(\mathbf{E} - \frac{\mathrm{tr}\,\mathbf{E}}{3}\mathbf{I}\right)$	0
References 33 and 36	$\mathbf{S} = 2\mu\left(\mathbf{D} - \frac{\mathrm{tr}\,\mathbf{D}}{3}\mathbf{I}\right)$	$\mathbf{S} = \left(\frac{2\mu_{\mathrm{p}}}{\lambda_1} - 2i\omega\mu_{\mathrm{s}}\right)\left(\mathbf{E} - \frac{\mathrm{tr}\,\mathbf{E}}{3}\mathbf{I}\right)$	0
Reference 34	$\mathbf{S} = 2\mu\mathbf{D} + \left(\mu_{\mathrm{B}} - \frac{2\mu_{\mathrm{s}}}{3}\right)(\mathrm{tr}\,\mathbf{D})\mathbf{I}$	N/A	$-\left(\mu_{\mathrm{B}} + \frac{2\mu_{\mathrm{p}}}{3}\right)(\boldsymbol{\nabla} \cdot \mathbf{v})$
Reference 35	$\mathbf{S} = 2\mu\left(\mathbf{D} - \frac{\mathrm{tr}\,\mathbf{D}}{3}\mathbf{I}\right)$	$\mathbf{S} = \frac{2\mu}{\lambda_1}\mathbf{E} + \frac{2i\omega\mu}{3}(\mathrm{tr}\,\mathbf{E})\mathbf{I}$	$\frac{2\mu}{3}\left(1 - \frac{1}{1-i\omega\lambda_1}\right)(\boldsymbol{\nabla} \cdot \mathbf{v})$
Reference 37	$\mathbf{S} = 2\mu\mathbf{D} + \left(\mu_{\mathrm{B}} - \frac{2\mu_{\mathrm{s}}}{3}\right)(\mathrm{tr}\,\mathbf{D})\mathbf{I}$	$\mathbf{S} = \left(\frac{2\mu_{\mathrm{p}}}{\lambda_1} - 2i\omega\mu_{\mathrm{s}}\right)\mathbf{E} + i\omega\left(\frac{2\mu_{\mathrm{s}}}{3} - \mu_{\mathrm{B}}\right)(\mathrm{tr}\,\mathbf{E})\mathbf{I}$	$-\left(\mu_{\mathrm{B}} + \frac{2\mu_{\mathrm{p}}}{3(1-i\omega\lambda_1)}\right)(\boldsymbol{\nabla} \cdot \mathbf{v})$
Equation (6) and Ref. 38	$\mathbf{S} = 2\mu\mathbf{D} + \left(\mu_{\mathrm{B}} - \frac{2\mu}{3}\right)(\mathrm{tr}\,\mathbf{D})\mathbf{I}$	$\mathbf{S} = 2G\mathbf{E} + \left(K - \frac{2G}{3}\right)(\mathrm{tr}\,\mathbf{E})\mathbf{I}$	$\frac{-\mu_{\mathrm{B}}\boldsymbol{\nabla}\cdot\mathbf{v}}{1-i\omega\lambda_{\mathrm{comp}}}$

III. APPLICATION OF CONSTITUTIVE EQUATION TO SPHERICAL AND BIPYRAMIDAL PARTICLES IMMERSED IN FLUID

In this section, we use the constitutive equation for a compressible viscoelastic fluid in Eq. (6) to examine the fluid-structure interaction of two example flows: (i) a spherical particle executing breathing mode oscillations in a fluid[17,26–28] and (ii) a bipyramidal particle undergoing extensional oscillations,[25] see schematic of particles in Fig. 1. The aim here is to demonstrate how mode shape and particle geometry affect the resulting flow dynamics. These solutions also find direct application in practice, because these particles are often measured using ultrafast laser spectroscopy to probe their dynamics.[17,25–28]

It has been established that nanometer-sized solid particles obey the continuum hypothesis[18,30] with their dynamics being governed by Navier's equation,

$$\rho_s \frac{\partial^2 \mathbf{u}}{\partial t^2} = \frac{E}{2(1+\sigma)} \left\{ \boldsymbol{\nabla}^2 \mathbf{u} + \frac{1}{(1-2\sigma)} \boldsymbol{\nabla}(\boldsymbol{\nabla} \cdot \mathbf{u}) \right\}, \tag{7}$$

where $\mathbf{u}$ is the displacement field, ρ_s is the solid density, E is the Young's modulus of the solid, and σ is the Poisson ratio. As before, we assume that the particle undergoes small-amplitude oscillations, and thus the usual assumption of linear elasticity is applicable. At the interface between the fluid domain and the solid particle, the conditions of continuity of stress, velocity, and displacement are imposed. This provides direct coupling between the linear compressible viscoelastic fluid, Eqs. (5) and (6), and Navier's equation for the solid, Eq. (7). At large distances from the particle, we require that all generated waves are outgoing.

Because the motion is oscillatory, all time-dependent variables, such as the solid displacement, fluid velocity, and fluid pressure, are expressed in terms of the explicit time dependence $e^{-i\omega t}$,

$$X(\mathbf{r}, t) = \tilde{X}(\mathbf{r}|\omega) e^{-i\omega t}, \tag{8}$$

where i is the usual imaginary unit, $\mathbf{r}$ is the position, ω is the angular frequency, and X denotes any time-dependent quantity. For simplicity, we henceforth omit the superfluous "~" notation, noting that the above relation holds universally for harmonic oscillations.

A. Spherical particles

An analytical solution can be found for the breathing mode oscillations of a sphere in an unbounded linear compressible viscoelastic fluid. Throughout, we assume that the deformation of the solid particle obeys the linear theory of elasticity. The breathing modes exhibit a pure radial displacement, i.e., $\mathbf{u}(\mathbf{r}) = u_r(r)\hat{\mathbf{r}}$, where r is the usual radial coordinate in spherical coordinates, $\hat{\mathbf{r}}$ is its corresponding basis vector, and $u_r(r)$ is the radial component. Therefore, the governing equation for the radial displacement of a sphere is

$$\frac{\mathrm{d}^2 u_r}{\mathrm{d}r^2} + \frac{2}{r}\frac{\mathrm{d}u_r}{\mathrm{d}r} - \frac{2u_r}{r^2} + \tau^2 u_r = 0, \tag{9}$$

where $\tau = \omega \sqrt{\rho_s (1+\sigma)(1-2\sigma)/E(1-\sigma)}$. The general solution to Eq. (9) yielding a finite solution at the origin is $u_r(r) = A j_1(\tau r)$, where $j_1(\tau r)$ is the spherical Bessel function of first kind and A is a constant. Since the particle executes breathing mode oscillations, the resulting velocity field in the fluid is

$$v_r = -i\omega \, u_r|_{r=R} \frac{k_1\left(-i\alpha \frac{r}{R}\right)}{k_1(-i\alpha)}, \tag{10}$$

where R is the particle radius and k_1 is the modified spherical Bessel function of second kind. The parameter α is defined as

$$\alpha^2 = \frac{\beta \varsigma^2 (1 - i\mathrm{De}_{\mathrm{sh}})}{\beta(1 - i\mathrm{De}_{\mathrm{sh}}) - i\varsigma^2 \left(\frac{4}{3} + \theta \frac{1 - i\mathrm{De}_{\mathrm{sh}}}{1 - i\mathrm{De}_{\mathrm{comp}}}\right)}, \tag{11}$$

where $\beta = \rho_0 \omega R^2/\mu$, $\varsigma = \omega R\sqrt{\rho_0 \kappa}$, $\theta = \mu_B/\mu$, $\text{De}_{\text{sh}} = \lambda_{\text{sh}}\omega$, and $\text{De}_{\text{comp}} = \lambda_{\text{comp}}\omega$; De is the Deborah number.

Continuity of stress and velocity is then imposed at the particle-fluid interface, at $r = R$, giving

$$\frac{E(1-\sigma)}{(1+\sigma)(1-2\sigma)}\left[\frac{du_r}{dr} + \frac{2\sigma}{(1-\sigma)}\frac{u_r}{r}\right]_{r=R}$$

$$= \left[-p + 2\frac{\mu}{(1-i\lambda_{\text{sh}}\omega)}\frac{dv_r}{dr} - \left(\frac{2\mu}{3(1-i\lambda_{\text{sh}}\omega)} - \frac{\mu_B}{(1-i\lambda_{\text{comp}}\omega)}\right)\left(\frac{dv_r}{dr} + \frac{2v_r}{r}\right)\right]_{r=R}. \tag{12}$$

Substituting the above-calculated displacement field for the solid, $u_r(r)$, and Eq. (10) into Eq. (12) yields the required eigenvalue equation for the complex eigenfrequency, ω. The angular resonant frequency, ω_f, in fluid is determined from this eigenfrequency,[40]

$$\omega_f = \sqrt{\omega_r^2 + \omega_i^2}, \tag{13}$$

where ω_r and ω_i are the real and imaginary components of ω, respectively.

The quality factor Q_{fluid}, which is a scaled rate of energy dissipation, is defined as the ratio of the maximum energy stored, E_{stored}, in the particle to the energy dissipated per cycle, E_{diss}, i.e., $Q_{\text{fluid}} = 2\pi (E_{\text{stored}}/E_{\text{diss}})|_{\omega=\omega_f}$. Its value can also be directly evaluated from ω,

$$Q_{\text{fluid}} = -\frac{\omega_f}{2\omega_i}, \tag{14}$$

where the subscript "fluid" indicates the contribution from the fluid only.

Following a similar approach to that adopted for a compressible viscoelastic fluid, an analytical solution can be derived for incompressible flow. However, the fluid velocity differs from the compressible solution and can be expressed as $v_r = -i\omega u_r|_{r=R}(R/r)^2$. Through continuity of stress and velocity at the solid-fluid interface, we arrive at the required complex eigenfrequency equation for the breathing modes in the incompressible fluid limit,

$$\tau R\left[1 + \frac{4i}{\beta(1-i\text{De}_{\text{sh}})}\right]j_1(\tau R) = \frac{\rho_s}{\rho}\left[j_0(\tau R) - \frac{2(1-2\sigma)}{(1-\sigma)\tau R}j_1(\tau R)\right], \tag{15}$$

where $j_n(\tau R)$ is the spherical Bessel function of first kind and ω is the complex eigenfrequency.

1. Numerical results

We now present the numerical results for the fundamental breathing mode vibration of a sphere immersed in a compressible viscoelastic fluid. The problem depends on several dimensionless variables as follows:

i. The effects of compressibility and viscoelasticity are controlled by separate dimensionless parameters: the normalized wave number ς and the Deborah numbers De_{sh} and De_{comp}, respectively. The latter indicate the strength of shear and compressional elasticities. Small values for all these parameters indicate a negligible effect of fluid compressibility and fluid elasticity.
ii. The normalized frequency β dictates the effect of shear viscosity, whereas the ratio of the bulk-to-shear viscosities is $\theta \equiv \mu_B/\mu$.
iii. The density ratio ρ_s/ρ specifies the relative strength of solid-to-fluid inertia and thus the strength of the fluid loading.

We consider solid-to-fluid density ratios, ρ_s/ρ, in the range 3–1000; the lower limit of this range is typical for semiconductor nanoparticles, whereas materials such as gold exhibit a density ratio of approximately 20—the upper limit of 1000 is studied to illustrate behavior in the high density ratio limit. For simplicity, Deborah numbers with $\text{De}_{\text{comp}} = \text{De}_{\text{sh}}$ and a viscosity ratio, $\mu_B/\mu = 1$, which are the good approximations for some real fluids, see Appendix A. Poisson's ratio is set to $\sigma = 0.44$, typical for gold. Throughout, a variable with subscript "f" refers to the variable evaluated at the resonant frequency in fluid, ω_f.

A Knudsen number can be defined from the above dimensionless parameters, $Kn = \varsigma^2/\beta$. For gases, this is proportional to the ratio of the gas mean free path and acoustic wavelength. The continuum approximation is observed when $Kn \ll 1$. Importantly, $\varsigma^2 \ll \beta$ implies that the time scale for vorticity diffusion is far smaller than the time scale for sound propagation. This is true regardless of the nature of the fluid. Therefore, $\varsigma^2 \ll \beta$ must be satisfied in both gases and liquids for the continuum approximation to hold. Flows with $\beta < 10$ require $\varsigma^2 \ll 10$ and are thus incompressible. As a result, the effects of fluid compressibility are expected in the high-β regime; this does not eliminate its effects for moderate or small β, as we shall discuss.

a. Effect of shear relaxation time. It is informative to isolate the effects of fluid compressibility and viscoelasticity in this numerical study. As such, the compressible viscoelastic solution is compared to the corresponding incompressible result at identical Deborah numbers. We first examine the effect of the Deborah number on the resonant frequency of the sphere. This is performed for a density ratio of $\rho_s/\rho = 20$, which is typical for gold nanoparticles.[30]

Figure 2(a) shows the resonant frequency as a function of normalized frequency, $\beta_f \equiv \rho \omega_f R^2/\mu$, for various Deborah numbers, De. Reducing β_f increases the fluid stress, which ultimately becomes comparable to the stress in the solid. This can strongly affect the mode shape and thus complicate mode identification, especially for the incompressible solution; results are given for large values of β_f only in these cases. As expected, the incompressible and compressible results coincide for low β_f, where significant departures from the Newtonian solution are observed. For large values of β_f, the compressible and incompressible results differ, in agreement with the scaling analysis above. This verifies that fluid compressibility is critical in the high β_f regime but produces a weak effect for small β_f.

Corresponding results for the quality factor are given in Fig. 2(b). Compressible and incompressible Newtonian theory (De = 0) predicts that the quality factor decreases monotonically with decreasing β_f. Again, we observe a difference between the compressible and incompressible results for large β_f, but coincidence for $\beta_f \lesssim 1$. The situation changes dramatically for finite De. First, results in Fig. 2(b) show that elasticity results in qualitatively different behavior in the low β_f-regime. Rather than a reduction in quality factor with decreasing β_f, the quality factor now increases monotonically; this is discussed further below. Interestingly, the value of β_f, where the compressible and incompressible results coincide, decreases with increasing De; this value of β_f is seen to be approximately given by $Min(1/De, 1)$. This is not surprising because $De_{sh} = De_{comp}$, and thus, increasing De simultaneously enhances the effects of compressional elasticity; since $De_{sh} \approx De_{comp}$ for some real fluids,[25] this effect should be observable experimentally.

The situation for $\beta_f > 1$ is strikingly different, with fluid compressibility producing a constant value in the quality factor as β_f increases while the incompressible solution gives a monotonically
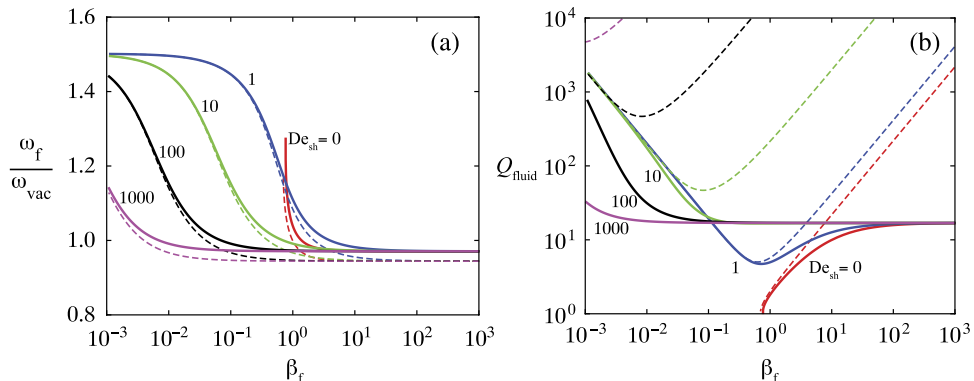
FIG. 2. Breathing mode vibration of a sphere immersed in a compressible viscoelastic fluid—effect of viscoelasticity and fluid compressibility. (a) Resonant frequency and (b) quality factor. Deborah number, De = 0 (red), 1 (blue), 10 (green), 100 (black), and 1000 (magenta). Results for density ratio $\rho_s/\rho = 20$, Poisson ratio $\sigma = 0.44$, viscosity ratio $\theta \equiv \mu_B/\mu = 1$, and Deborah numbers are chosen so that $De_{comp} = De_{sh}$ and a normalized wavenumber $\varsigma = 1$. Compressible fluids (solid lines); Incompressible fluids (dashed lines).

increasing quality factor. This difference is due to the radiation of sound waves in the compressible result, which restricts the upper value of the quality factor in the inviscid limit, i.e., $\beta_\mathrm{f} \to \infty$.

b. Relation to the elasticity number. The elasticity number, $\mathrm{El} \equiv \mathrm{De}/\beta = \mu\lambda/(\rho R^2)$, is often used in rheology because it depends only on the fluid material properties and the device geometry—the excitation frequency, ω_f, is eliminated. A higher value for this parameter denotes a stronger viscoelastic effect. Use of this parameter, rather than the Deborah number, is particularly advantageous in conventional rheology because the device geometry is often fixed and the excitation frequency is adjusted independently. For a vibrating nanoparticle, however, this is not possible because its resonant frequency is directly connected to its size; the frequency can only be adjusted by changing the particle size (radius R for a sphere)—varying β_f immediately results in a change in El. Nonetheless, we note that results in Fig. 2, when plotted as a function of El rather than De, display near identical behavior.

c. Effect of density ratio. Next, we examine the effect of the density ratio, ρ_s/ρ, and normalized frequency, β_f, on the dynamic response. The normalized frequency, β_f, is the squared ratio of the particle radius to the viscous penetration depth and therefore, dictates the effect of the shear viscosity. The density ratio, ρ_s/ρ, specifies the relative strength of solid and fluid inertia. Increasing both parameters, β_f and ρ_s/ρ, reduces the effect of fluid viscosity and fluid inertia—in the binary limit, $\beta_\mathrm{f} \to \infty$ and $\rho_\mathrm{s}/\rho \to \infty$, energy dissipation and fluid inertia are eliminated, with the resonant frequency matching the result in vacuum, ω_vac, and the quality factor rising unboundedly. This removes the effect of the surrounding fluid.

In Fig. 3, we present results for the resonant frequency and quality factor of a sphere in a compressible Newtonian ($\mathrm{De_{sh}} = \mathrm{De_{comp}} = 0$) and a viscoelastic fluid. Results in Fig. 3(a) clearly show that viscoelasticity dramatically affects the resonant frequency, especially for small β_f. In contrast to the Newtonian result for small β_f, shear elasticity in the fluid can strongly enhance the resonant frequency. The underlying physical mechanism lies in storage of elastic energy in the fluid, which adds directly to the energy stored in the solid particle. This stiffens the particle/fluid system, resulting in the observed resonant frequency increase. Interestingly, we find that in the asymptotic limit of infinite viscosity (zero inertia), i.e., $\beta_\mathrm{f} \to 0$, the resonant frequency enhancement plateaus to a constant value of $\omega_\mathrm{f}/\omega_\mathrm{vac} = 1.5$. This feature should be observable experimentally and may provide a useful experimental route to identifying the presence of fluid viscoelasticity. At high β_f, fluid loading is dominated by a compressible inviscid contribution—a reduction in ρ_s/ρ enhances the effect of the surrounding fluid on the particle dynamics, leading to a decrease in the resonant frequency.

Behavior strikingly different from the Newtonian result is again observed for the quality factor, in the low inertia limit. While Newtonian considerations would indicate that the quality factor should predominantly decrease with a reduction in β_f, the complete viscoelastic results show the
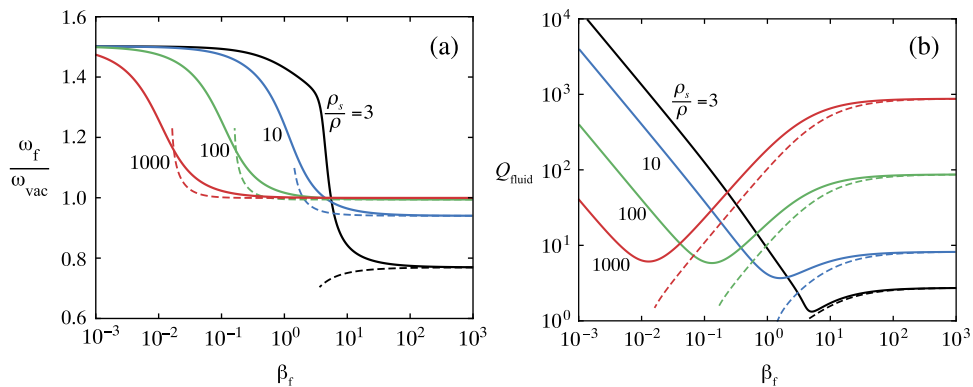

FIG. 3. Breathing mode vibration of a sphere immersed in a compressible viscoelastic fluid—effect of density ratio ρ_s/ρ. (a) Resonant frequency and (b) quality factor. Density ratios $\rho_\mathrm{s}/\rho = 3$ (black), 10 (blue), 100 (green), and 1000 (red). $\mathrm{De_{sh}} = 1$ (solid lines) and $\mathrm{De_{sh}} = 0$ (dashed lines). Poisson ratio $\sigma = 0.44$, viscosity ratio $\theta \equiv \mu_\mathrm{B}/\mu = 1$, Deborah numbers $\mathrm{De_{comp}} = \mathrm{De_{sh}}$, and a normalized wavenumber $\varsigma = 1$.

opposite trend. For low β_f, the quality factor increases with an enhancement in viscosity, following an asymptotic trend: $Q_{\text{fluid}} \propto 1/\beta_f$. The mechanism for this seemingly unintuitive behavior is identical to that observed for the resonant frequency: enhancement in energy dissipation, as β_f is reduced, is overly compensated by greater energy storage in the particle/fluid system—this leads to the observed increase in the quality factor with decreasing β_f. For high β_f, the predominantly compressible inviscid flow gives a reduction in quality factor with decreasing ρ_s/ρ.

d. Implications to mass sensing using nanomechanical sensors. The results in Fig. 3(b) show that operation at lower ρ_s/ρ can result in higher quality factors at low β_f. This is contrary to current thinking and has significant implications in practice. For example, mechanical sensors are presently being used widely to detect minute masses with molecular and atomic resolutions in vacuum. Operation in liquid remains a significant challenge. Importantly, a reduction in β_f coincides with a uniform reduction in device size. The presented results therefore indicate that miniaturization of low-density solid particles may provide an ideal platform for such sensing applications in liquid, allowing for improved mass sensitivity through reduction in device mass and enhancement in quality factor. This suggests that the natural viscoelastic response of simple liquids may be used advantageously to perform such highly sensitive measurements at nanometer scales.

e. Effect of fluid compressibility and bulk viscosity. The effect of the fluid bulk viscosity is controlled predominantly by the normalized wavenumber ς. The flow is incompressible and the bulk viscosity has no effect, if $\varsigma \ll 1$. Operation at finite ς can lead to a rich interplay between the bulk viscosity and the elastic relaxation properties of the fluid. This is especially the case for high β_f, where the effects of fluid compressibility are strong. Varying the ratio of De_{comp} and De_{sh} also modifies the behavior, as expected (data not shown). Operation at high Deborah number increases the effect of fluid compressibility and bulk viscosity, leading to enhanced compressibility effects at low β_f, similar to that observed in Fig. 2.

The presented results and discussion show that the combined effects of fluid compressibility and viscoelasticity can critically affect the dynamics of spherical nanoparticles immersed in simple liquids.

B. Bipyramidal particles

The impact of fluid compressibility is strongly controlled by the particle geometry and vibration mode. To illustrate this aspect, we now examine the extensional mode vibrations of bipyramidal particles in fluid, which were reported in Ref. 25. This previous study measured the dynamic response of gold bipyramidal nanoparticles immersed in glycerol-water mixtures as a function of glycerol-water mass fraction. Increasing the glycerol mass fraction simultaneously enhances the viscosity, μ, and relaxation time, λ, of the liquid, resulting in a multiplicative enhancement in the elasticity number, $\text{El} = \mu\lambda/(\rho R^2)$—and thus liquid elasticity; R refers to the maximum radius of the bypyramid here.[25] These measurements were compared to a theoretical model based on an incompressible linear viscoelastic fluid model, for which excellent agreement was observed. Incompressible flow is expected because the particle extensional mode predominantly generates shear waves in the surrounding fluid. Here, we provide complementary theoretical results that rigorously include the effects of fluid compressibility, using Eq. (6), to assess the validity of this assumption. Material properties of the gold nanoparticle and glycerol-water mixtures are reported in Appendix A. The fluid-structure problem, defined in Eqs. (5)–(7), is solved using a fully coupled finite-element (FE) fluid-structure simulation;[44] validation of this finite-element solution using the analytical solution for a spherical particle is given in Appendix B.

Figure 4 shows the results of this numerical simulation for both incompressible[25] and compressible flows. From these results, it is clear that fluid compressibility exerts a weak effect on both the resonant frequency and quality factor of the particle. This comparison verifies that fluid compressibility does not significantly affect the dynamics of bipyramidal particles undergoing extensional mode vibrations, in contrast to the case of a spherical particle executing breathing mode oscillations, presented above. As such, the compressible model in Eq. (6) encompasses the general case
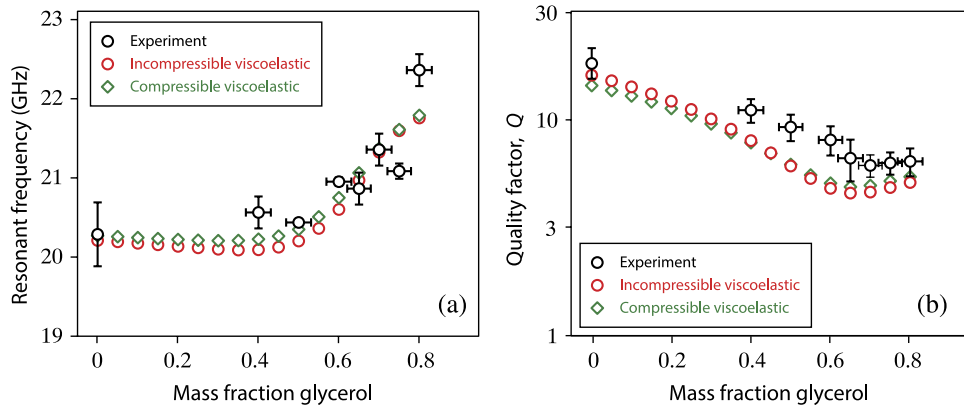
FIG. 4. Bipyramidal particle undergoing extensional model vibrations in glycerol-water mixtures.[25] (a) Resonant frequency and (b) Quality factor. Experimental data (black circles with error bars);[25] incompressible viscoelastic FE calculations (red circles);[25] Compressible viscoelastic FE calculations (green diamonds). FE calculations assume a quality factor due to intrinsic damping, $Q_{int} = 50$. The total quality factor due to the fluid and intrinsic damping is given, $1/Q = 1/Q_{fluid} + 1/Q_{int}$.

and can be used to calculate the flows generated by arbitrarily shaped nanoscale devices immersed in simple liquids.

IV. CONCLUSIONS

We have examined the available constitutive equations for linear compressible viscoelastic fluids, and showed that only Eq. (6) is consistent with classical thermodynamic results. The underlying physical mechanisms of this model were discussed. This model exhibits all the required features of a linear viscoelastic flow, with fluid-like behavior at frequencies well below the characteristic relaxation times and solid-like behavior at high frequencies. This is in direct contrast to other constitutive models for compressible viscoelastic flows,[32–37] which do not possess the correct limiting behavior at high frequency. Exploration of the validity of these constitutive equations is motivated by recent measurements showing that the natural viscoelastic response of simple liquids critically affects the dynamic response of vibrating nanostructures.

The utility of the constitutive equation in Eq. (6) was demonstrated by analyzing the fluid-structure interaction of particles with different geometries and mode shapes: spherical and bipyramidal particles. These particles are commonly measured in practice. Spherical particles executing breathing mode oscillations were found to generate compressible flows, with strong interplay between the effects of fluid compressibility, bulk viscosity, and fluid relaxation processes. In contrast, the extensional mode vibrations of bipyramidal particles inherently generate incompressible viscoelastic flows. The constitutive equation in Eq. (6) handles both cases naturally and thus, provides a general formalism with which to characterize the fluid-structure interaction of nanoscale mechanical devices vibrating in simple liquids. This is expected to be particularly useful in interpreting current measurements that interrogate the picosecond dynamics of vibrating nanoparticles using ultrafast laser spectroscopy.[30]

ACKNOWLEDGMENTS

APPENDIX A: MATERIAL PROPERTIES

1. Gold nanoparticles

Gold nanoparticles are considered to have bulk material properties: density of 19 320 kg/m^3, Young's modulus of 79 GPa, and a Poisson's ratio of 0.44.
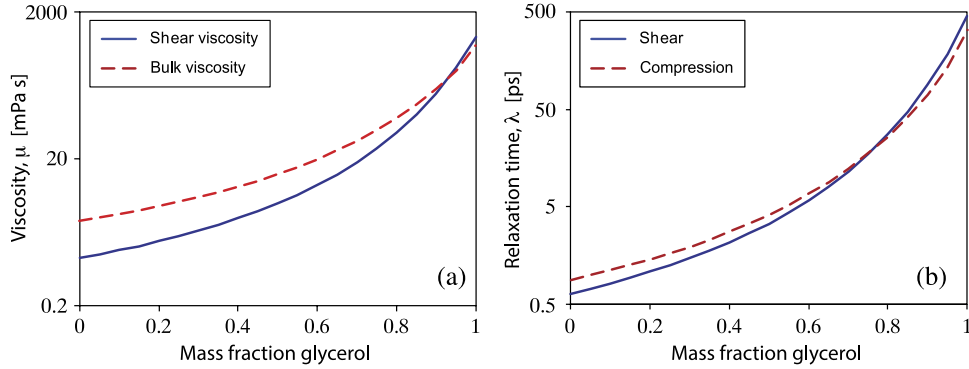
FIG. 5. Shear and compressional (bulk) components of (a) viscosity and (b) relaxation time, as a function of glycerol mass fraction, for glycerol/water mixtures at 25 °C.

2. Glycerol-water mixtures

A standard temperature dependent empirical formula[45] is used to calculate the low-frequency shear viscosities of water-glycerol mixtures. Both shear and compression relaxation times are specified by the ultrasonic measurements of Slie *et al.*[46] These two relaxation times are given by

$$\lambda_{\text{sh}} = \frac{\mu}{G_\infty}, \qquad \lambda_{\text{comp}} = \frac{\mu_B}{K_2}, \tag{A1}$$

where G_∞ is the high-frequency shear modulus, K_2 is the difference between the high-frequency bulk modulus, K_∞, and the low-frequency or static bulk modulus, K_0. Slie *et al.*[46] show that both G_∞ and K_2 vary linearly with glycerol concentration and temperature. Performing a linear regression on these parameters gives

$$G_\infty = (2.6787 - 0.9929\, c_{\text{m}}) - (0.0276 - 0.0154\, c_{\text{m}})\, T \quad [\text{GPa}], \tag{A2}$$

$$K_\infty - K_0 = (3.0528 + 0.6244\, c_{\text{m}}) - (0.0339 - 0.0133\, c_{\text{m}})\, T \quad [\text{GPa}], \tag{A3}$$

where c_{m} is the mole fraction of water and T is the temperature in °C. Figure 5 shows the resulting dependence of the shear and bulk viscosities, μ and μ_B, and relaxation times, λ_{sh} and λ_{comp}, on the mass fraction of glycerol, for water-glycerol mixtures at 25 °C.

The limiting values for the shear and compression relaxation times predicted by Eqs. (A2) and (A3) agree with independent reports for water and pure glycerol.[47,48]

APPENDIX B: VALIDATION OF FINITE-ELEMENT CALCULATIONS

In this Appendix, we validate the finite-element fluid structure calculations using the exact solution for a spherical particle undergoing breathing mode oscillations in a compressible viscoelastic fluid (Sec. III A).

The coupled system of equations, Eqs. (5)–(7), is solved using the commercial finite-element software COMSOL Multiphysics, using its eigenfrequency solver.[44] Equations (5) and (7) are implemented by modifying the weak form of COMSOL's fluid-structure interaction module. Because equations for the extra viscoelastic stresses, i.e., shear and compression, are not readily available in this software, weak forms of Eq. (6) are implemented using its partial differential equation (PDE-mode) solver. We use the same boundary conditions as in the analytical model for the spherical particles described in Sec. III A. At boundaries far from the particle, the outgoing boundary condition for a generated wave is applied. A schematic of the computational domain is given in Fig. 6. Because the flow and particle deformations are axisymmetric, the domain is restricted to the *r*-*z* plane. The fluid is chosen to be a glycerol-water mixture, and the particle material is gold, whose material properties are given in Appendix A. The reported results are independent of mesh size and domain size to within 0.1%.
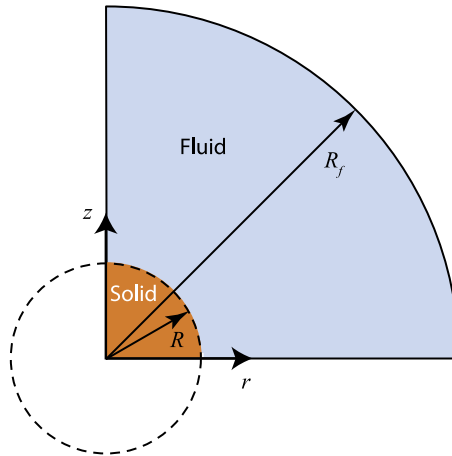
FIG. 6. Schematic of a spherical particle immersed in fluid, showing the computational domain and particle dimension. Fluid region (blue) and solid region (gold). Radial extent of fluid computational domain is R_f.
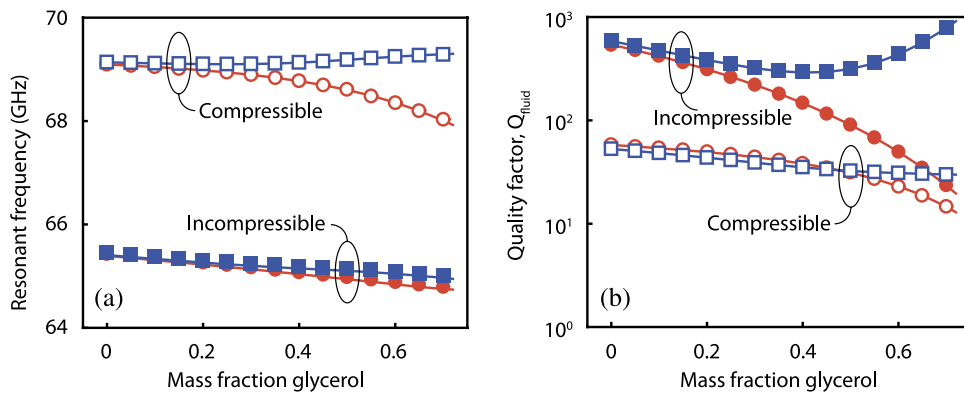

FIG. 7. Spherical particle of diameter 50 nm immersed in glycerol/water mixtures at 20 °C. Particle is undergoing breathing mode oscillations. (a) Resonant frequency and (b) Quality factor. Analytical solutions (lines) pass precisely through the corresponding finite-element results (symbols). Newtonian (red circles); viscoelastic (blue squares); incompressible (filled symbols); and compressible (open symbols).

Figure 7 shows a comparison between the exact analytical solution and results of the FE analysis. Excellent agreement is found over the entire parameter range considered, with the results obtained of these independent approaches being indistinguishable. This validates the FE simulations that are used to calculate the dynamics of the bipyramidal particles in Sec. III B.

[1] J. S. Bunch, A. M. van der Zande, S. S. Verbridge, I. W. Frank, D. M. Tanenbaum, J. M. Parpia, H. G. Craighead, and P. L. McEuen, "Electromechanical resonators from graphene sheets," Science **315**, 490 (2007).

[2] T. P. Burg, M. Godin, S. M. Knudsen, W. Shen, G. Carlson, J. S. Foster, K. Babcock, and S. R. Manalis, "Weighing of biomolecules, single cells and single nanoparticles in fluid," Nature **446**, 1066 (2007).

[3] H.-Y. Chiu, P. Hung, H. W. C. Postma, and M. Bockrath, "Atomic-scale mass sensing using carbon nanotube resonators," Nano Lett. **8**, 4342 (2008).

[4] N. V. Lavrik, M. J. Sepaniak, and P. G. Datskos, "Cantilever transducers as a platform for chemical and biological sensors," Rev. Sci. Instrum. **75**, 2229 (2004).

[5] M. L. Juan, M. Righini, and R. Quidant, "Plasmon nano-optical tweezers," Nat. Photonics **5**, 349 (2011).

[6] K. Jensen, K. Kim, and A. Zettl, "An atomic-resolution nanomechanical mass sensor," Nat. Nanotechnol. **3**, 533 (2008).

[7] H. B. Peng, C. W. Chang, S. Aloni, T. D. Yuzvinsky, and A. Zettl, "Ultrahigh frequency nanotube resonators," Phys. Rev. Lett. **97**, 087203 (2006).

[8] A. K. Naik, M. S. Hanay, W. K. Hiebert, X. L. Feng, and M. L. Roukes, "Towards single-molecule nanomechanical mass spectrometry," Nat. Nanotechnol. **4**, 445 (2009).

[9] Y. T. Yang, C. Callegari, X. L. Feng, K. L. Ekinci, and M. L. Roukes, "Zeptogram-scale nanomechanical mass sensing," Nano Lett. **6**, 583 (2006).

[10] J. L. Arlett and M. L. Roukes, "Ultimate and practical limits of fluid-based mass detection with suspended microchannel resonators," J. Appl. Phys. **108**, 084701 (2010).

[11] J. L. Arlett, E. B. Myers, and M. L. Roukes, "Comparative advantages of mechanical biosensors," Nat. Nanotechnol. **6**, 203 (2011).

[12] A. Eichler, J. Moser, J. Chaste, M. Zdrojek, I. Wilson Rae, and A. Bachtold, "Nonlinear damping in mechanical resonators made from carbon nanotubes and graphene," Nat. Nanotechnol. **6**, 339 (2011).

[13] P. Zijlstra, P. M. R. Paulo, and M. Orrit, "Optical detection of single non-absorbing molecules using the surface plasmon resonance of a gold nanorod," Nat. Nanotechnol. **7**, 379 (2012).

[14] M. H. Matheny, L. G. Villanueva, R. B. Karabalin, J. E. Sader, and M. L. Roukes, "Nonlinear mode-coupling in nanomechanical systems," Nano Lett. **13**, 1622 (2013).

[15] J. H. Hodak, A. Henglein, and G. V. Hartland, "Size dependent properties of Au Particles: Coherent excitation and dephasing of acoustic vibrational modes," J. Chem. Phys. **111**, 8613 (1999).

[16] C. Voisin, N. Del Fatti, D. Christofilos, and F. Vallée, "Time-resolved investigation of the vibrational dynamics of metal nanoparticles," Appl. Surf. Sci. **164**, 131 (2000).

[17] M. Hu, X. Wang, G. V. Hartland, P. Mulvaney, J. P. Juste, and J. E. Sader, "Vibrational response of nanorods to ultrafast laser induced heating: Theoretical and experimental analysis," J. Am. Chem. Soc. **125**, 14925 (2003).

[18] V. Juvé, A. Crut, P. Maioli, M. Pellarin, M. Broyer, N. Del Fatti, and F. Vallée, "Probing elasticity at the nanoscale: Terahertz acoustic vibration of small metal nanoparticles," Nano Lett. **10**, 1853 (2010).

[19] D. G. Crighton, "Resonant oscillations of fluid-loaded struts," J. Sound Vib. **87**, 429 (1983).

[20] S. Basak, A. Raman, and S. V. Garimella, "Hydrodynamic loading of microcantilevers vibrating in viscous fluids," J. Appl. Phys. **99**, 114906 (2006).

[21] J. E. Sader, "Frequency response of cantilever beams immersed in viscous fluids with applications to the atomic force microscope," J. Appl. Phys. **84**, 64 (1998).

[22] R. J. Clarke, S. M. Cox, P. M. Williams, and O. E. Jensen, "The drag on a microcantilever oscillating near a wall," J. Fluid Mech. **545**, 397 (2005).

[23] J. W. M. Chon, P. Mulvaney, and J. E. Sader, "Experimental validation of theoretical models for the frequency response of atomic force microscope cantilever beams immersed in fluids," J. Appl. Phys. **87**, 3978 (2000).

[24] C. Cercignani, *Rarefied Gas Dynamics: From Basic Concepts to Actual Calculation* (Cambridge University Press, Cambridge, UK, 2000).

[25] M. Pelton, D. Chakraborty, E. Malachosky, P. Guyot-Sionnest, and J. E. Sader, "Viscoelastic flows in simple liquids generated by vibrating nanostructures," Phys. Rev. Lett. **111**, 244502 (2013).

[26] M. Pelton, J. E. Sader, J. Burgin, M. Z. Liu, P. Guyot-Sionnest, and D. Gosztola, "Damping of acoustic vibrations in gold nanoparticles," Nat. Nanotechnol. **4**, 492 (2009).

[27] P. V. Ruijgrok, P. Zijlstra, A. L. Tchebotareva, and M. Orrit, "Damping of acoustic vibrations of single gold nanoparticles optically trapped in water," Nano Lett. **12**, 1063 (2012).

[28] T. A. Major, A. Crut, B. Gao, S. S. Lo, N. D. Fatti, F. Vallee, and G. V. Hartland, "Damping of the acoustic vibrations of a suspended gold nanowire in air and water environments," Phys. Chem. Chem. Phys. **15**, 4169 (2013).

[29] J. C. Maxwell, "On the dynamical theory of gases," Philos. Trans. R. Soc. London **157**, 49 (1867).

[30] G. V. Hartland, "Optical studies of dynamics in noble netal nanostructures," Chem. Rev. **111**, 3858 (2011).

[31] R. B. Bird, R. C. Armstrong, and O. Hassager, *Dynamics of Polymeric Liquids* (John Wiley and Sons Inc., New York, NY, USA, 1987).

[32] B. J. Edwards and A. N. Beris, "Remarks concerning compressible viscoelastic fluid models," J. Non-Newtonian Fluid Mech. **36**, 411 (1990).

[33] I. J. Keshtiban, F. Belblidia, and M. F. Webster, "Numerical simulation of compressible viscoelastic liquids," J. Non-Newtonian Fluid Mech. **122**, 131 (2004).

[34] Š. Matušů-Nečasová, A. Sequeira, and J. H. Videman, "Existence of classical solutions for compressible viscoelastic fluids of Oldroyd type past an obstacle," Math. Methods Appl. Sci. **22**, 449 (1999).

[35] R. Sureshkumar, "Stability analysis using compressible viscoelastic formulation," J. Non-Newtonian Fluid Mech. **116**, 471 (2004).

[36] K. D. Housiadas and G. C. Georgiou, "Perturbation solution of Poiseuille flow of a weakly compressible Oldroyd-B fluid," J. Non-Newtonian Fluid Mech. **166**, 73 (2011).

[37] S. J. Lind and T. N. Phillips, "Bubble collapse in compressible fluids using a spectral element marker particle method. Part 2. Viscoelastic fluids," Int. J. Numer. Methods Fluids **71**, 1103 (2013).

[38] W.-A. Yong, "Newtonian limit of Maxwell fluid flows," Arch. Ration. Mech. Anal. **214**, 913 (2014).

[39] L. D. Landau and E. M. Lifshitz, *Fluid Mechanics* (Pergamon, Oxford, 1959).

[40] D. Chakraborty, E. van Leeuwen, M. Pelton, and J. E. Sader, "Vibration of nanoparticles in viscous fluids," J. Phys. Chem. C **117**, 8536 (2013).

[41] J. F. Brady, A. S. Khair, and M. Swaroop, "On the bulk viscosity of suspensions," J. Fluid Mech. **554**, 109 (2006).

[42] G. K. Batchelor, *An Introduction to Fluid Dynamics* (Cambridge University Press, Cambridge, UK, 1967).

[43] C. Klieber, T. Hecksher, T. Pezeril, D. H. Torchinsky, J. C. Dyre, and K. A. Nelson, "Mechanical spectra of glass-forming liquids. II. Gigahertz-frequency longitudinal and shear acoustic dynamics in glycerol and DC704 studied by time-domain Brillouin scattering," J. Chem. Phys. **138**, 12A544 (2013).

[44] COMSOL, *COMSOL Multiphysics User's Guide* (COMSOL, Burlington, MA, USA, 2008).

[45] N.-S. Cheng, "Formula for the viscosity of a glycerol–water mixture," Ind. Eng. Chem. Res. **47**, 3285 (2008).

[46] W. M. Slie, J. A. R. Donfor, and T. A. Litovitz, "Ultrasonic shear and longitudinal measurements in aqueous glycerol," J. Chem. Phys. **44**, 3712 (1966).

[47] R. Piccirelli and T. A. Litovitz, "Ultrasonic shear and compressional relaxation in liquid glycerol," J. Acoust. Soc. Am. **29**, 1009 (1957).

[48] G. D'Arrigo, "Sound propagation in moderately supercooled liquids. A comparison with water," J. Chem. Phys. **75**, 921 (1981).